Evaluation of Hydrogen-Deuterium Exchange during Transient Vapor Binding of MeOD with Model Peptide Systems Angiotensin II and Bradykinin

Authors: Haley M. Schramm,[1] Tomoya Tamadate,[2] Christopher J. Hogan,[2] Brian H. Clowers[1]*

[1]Department of Chemistry, Washington State University, Pullman, WA 99163, USA

[2]Department of Mechanical Engineering, University of Minnesota, Minneapolis, MN 55455, USA

* Corresponding Author: Brian H. Clowers, brian.clowers@wsu.edu, 509-335-4300

Abstract:

The advancement of hybrid mass spectrometric tools as an indirect probe of molecular structure and dynamics relies heavily upon a clear understanding between gas-phase ion reactivity and ion structural characteristics. This work provides new insights into gas-phase ion-neutral reactions of the model peptides (i.e., angiotensin II and bradykinin) on a per-residue basis by integrating hydrogen/deuterium exchange, ion mobility, tandem mass spectrometry, selective vapor binding, and molecular dynamics simulations. By comparing fragmentation patterns with simulated probabilities of vapor uptake, a clear link between gas-phase hydrogen/deuterium exchange and the probabilities of localized vapor association is established. The observed molecular dynamics trends related to the sites and duration of vapor binding track closely with experimental observation. Additionally, the influence of additional charges and structural characteristics on exchange kinetics and ion-neutral cluster formation is examined. These data provide a foundation for the analysis of solvation dynamics of larger, native-like conformations of proteins in the gas phase.

Keywords: Ion Mobility Spectrometry; Hydrogen-Deuterium Exchange; Molecular Dynamics; Ion-Neutral Clustering

Introduction

Control of gas-phase ion chemistry remains a key factor in developing mass spectrometric techniques and strategies to probe gas-phase ion structures and dynamics. Moreover, tandem mass spectrometry and its numerous variants (e.g., collision-induced dissociation, charge transfer dissociation mechanisms, and radical-driven dissociation) rely extensively on the chemical nature of the target analyte and, in some cases, the surrounding environment.[1–10] Broadly, the field of gas-phase ion chemistry encompasses efforts aimed at identifying analyte charge locations before and during mass analysis.[1,2,4,11,12] Gas-phase hydrogen-deuterium exchange (gHDX) reactions are a unique class of experiments that provide constructive insights related to chemical reactivity and ion structure.[13–20] Physical measurements of ion behavior (e.g., *m/z*, ion-mobility (K), spectroscopic evaluations, and fragmentation patterns) serve to constrain experiments aimed at interpreting ion structure.[5,21–24] However, the inclusion of gas-phase reactivity and sites of chemical modification offer additional dimensions that broadly inform the dynamic natures of ion structure.

Initial gHDX experiments relied upon controlled leaks of deuterated gas into trapping mass spectrometers and recorded the evolution of isotopic envelopes as a function of time.[13,25–27] Although extended storage times were required and increasing the pressure of the trap broadly contradicts the goals of mass analyzers, early success was realized with impressive levels of deuterium incorporation similar to the solution-phase HDX experiments. For example, cytochrome c, when exposed to deuterated water in an ICR trap, exchanged 94% of the theoretically exchangeable hydrogens and allowed for at least three different conformers (on the basis of different reaction kinetics) to be identified with trapping times in excess of 1000 seconds.[13]

Previous work has also illustrated that the same amino acid residue in different locations within a peptide chain may exhibit different exchange kinetics due to three-dimensional structural effects or localized gas-phase basicity. Green and Lebrilla observed this behavior for bradykinin in the presence of deuterated water (D_2O) and suggested that the exchange proceeded through a relay mechanism.[27] According to Wyttenbach and Bowers, the surface accessibility of basic sites and the distance between them are what affect the observed rates for bradykinin and D_2O as determined by molecular dynamics.[28] One of the most significant conclusions from that work was that the experimental data could be accurately fit by using 25 conformers of bradykinin illustrating the dynamic nature of even small peptides in the gas phase.

Performing the HDX experiment within a mobility cell is appealing as it combines a chemical probe of accessible surfaces (gHDX) with a physical separation technique based on the orientationally averaged interactions between an ion and neutral.[14,29–31] In select cases, gHDX can be used to differentiate ion populations based on kinetics and deuterium incorporation to introduce an added dimension for characterization.[13,14,32] While these metrics can be used to infer dynamics and structure, ion mobility offers experimental results measuring the effects of charge and momentum-transfer ion-neutral cross-sections on the arrival time distributions of ion populations.[33] Valentine and Clemmer first reported gHDX experiments within a drift tube experiment and were able to identify shape-resolved conformers of cytochrome c.[14] By combining changes in the ion-neutral collisional cross-section and deuterium incorporation, they rationalized a broad array of ion characteristics based upon the degree of molecular charging. In their experiments, the more highly charged species displayed increased levels of deuterium incorporation due to elevated levels of surface accessibility and provided further experimental evidence of charge-induced elongation of gas-phase proteins, though the additional charges may also have influenced greater vapors sequestered resulting in increased exchange. More recently, Valentine et al. have developed a host of tools, including identifying changes in helicity, top-down structural identification, and ‘omics studies.[17,34–38]

The model peptides, angiotensin II and bradykinin have been studied extensively with a variety of deuterium sources and pressures. Freitas et al. studied a suite of these peptides and their derivatives and found that angiotensin II exchanged faster and more completely than bradykinin did with D_2O.[39] After 1 hour of storage with D_2O in an ICR, angiotensin II exchanged 13 Hs. While several other works evaluated different sources of deuterium, methanol-OD (CH_3OD or MeOD) has been shown to cluster selectively with single amino acids and achieve appreciable levels of exchange.[31] Lower pressure works using FT-ICRs with bradykinin $[M+2H]^{+2}$ showed 3 exchanges of hydrogen for deuterium at extended trapping times.[15,27,40] While initially quite successful, challenges with trapping ions for extended periods of time and measuring trace partial pressures of deuterating agents limited the broad adaptations of the technique as an indirect structural probe.

The introduction of condensable vapor phase species which form non-covalent ion-neutral complexes with analytes can also be employed in ion mobility-mass spectrometry (IM-MS) as a means to shift mobilities in an analyte-specific manner.[41–45] This adds further dimensionality to ion mobility experiments and can also be used as a means to probe gHDX. Angiotensin II, in addition to being a reportedly fast-exchanging peptide, has been studied in the context of ion-neutral clustering with alcohols. Efforts by Rawat et al. reported shifts in angiotensin II mobility as a function of the increased vapor pressure of isopropyl alcohol and attributed this behavior to site-specific vapor uptake.[46] More recently, using singly charged amino acid ions, we utilized MeOD as a dopant within an atmospheric pressure ion mobility drift cell to demonstrate a strong correlation between the degree of ion-neutral cluster formation and the extent of gHDX.[31] Such experiments build upon a framework put forward in prior studies showing that condensable vapor molecules transiently bind to analyte ions as they migrate in a drift cell. Because gas-phase chemistry retains the pertinent features of solution phase processes, gas-phase ions exposed to condensable vapors are in dynamic equilibrium (i.e., vapor molecules are continuously sorbing and desorbing as the ion migrates). Most importantly, changes in ion mobility arrival times when using condensable vapors directly correlate with the degree of ion-neutral clustering.[41] By simultaneously examining mobility shifts due to ion-neutral complex formation and the extent of gHDX via mass spectrometry, we observed that the rate of HDX appeared to decrease with an increased extent of MeOD conjugation with the amino acid ions, which was rationalized based on the steric hindrances to additional gHDX caused by the clustering neutral molecules.

This finding, coupled with prior studies of gHDX in lower pressure systems without long-lived ion-neutral cluster formation, suggests that the ions within the clusters have distinct gas phase behavior compared to their bare analyte counterparts, but the extent to which this conclusion can be generalized remains unclear. Here, we expand upon measurements using single amino acids to examine how condensable vapor clustering impacts gHDX exchangeable hydrogens with singly and doubly charged peptide ions, angiotensin II and bradykinin. In expanding measurements to larger ions, we explicitly probe (1) how charge states influence both the extent of ion-neutral complex formation and the extent of HDX, and (2) whether the ion-neutral complex formation also has a measurable impact on the rate of HDX for larger ions, which can accommodate multiple neutral adducts. Additionally, the experimental efforts are supported by a new molecular dynamics (MD) framework that explicitly accounts for ion-neutral cluster formation and mobility shifts due to transient clustering. From these simulations, the locations on the ions where clustered neutral molecules reside can be mapped onto the peptides on a per-residue basis providing a measurement for the probability of each amino acid sequestering a neutral vapor.

Methods

Sample Preparation. The model peptides bradykinin and angiotensin II were purchased from Sigma Aldrich. Stock solutions were prepared by reconstituting the lyophilized peptide in deionized water and stored at 5 °C. Working electrospray solutions were prepared fresh daily from the sock solutions using methanol with 0.1% formic acid to 50 μM for the peptides. Tetradodecyl ammonium (T12A) was included at 1 μM as a system suitability check for ion mobility calculations. This was done to ensure all variability in the mobility domain was of a chemical nature rather than instrumental drift or environmental factors. Over the concentration range used in this experiment, no HDX or shift in mobility was observed for T12A. For each replicate, the mobility for T12A was calculated to be 0.61 ± 0.1 $cm^2 V^{-1} s^{-1}$ or was otherwise thrown out and recollected.

Table 1 summarizes the analyte ions examined in this work. Only the $[M+2H]^{+2}$ ions of bradykinin were detected when sprayed from MeOH with 0.1% formic acid. Both the $[M+2H]^{+2}$ and $[M+H]^{+}$ ions for angiotensin II were observed in the mass spectra and used for analysis. The number of exchangeable hydrogens comes from the neutral molecule assuming HDX will proceed through a relay mechanism and exchange sites only capable of forming a hydrogen bond (see Figures S1 and S2). Protonation to form ions increases the number of exchangeable hydrogens by the number of charges added. The simulated charge locations were assigned based on individual amino acid basicity. The singly charged angiotensin II species was protonated at the Arg^2 residue only.

Analyte	Mass (g/mol)	z Detected	M^0 # of $H_{exchangeable}$	Amino Acid Sequence	Simulated Charge Locations
Bradykinin	1060	2	17	RPPGFSPFR	Arg^1, Arg^9
Angiotensin II	1046	1, 2	16	DRVYIHPF	Arg^2, Pro^7
T12A	691	1	0	n/a	n/a

Table 1: Analyte information.

Ion-Mobility Mass Spectrometry. Gas-phase HDX during transient vapor binding was performed as explained previously.[31] Working solutions were electrosprayed at 3 μL/min into the

IMS using a 75 μm ID glass capillary using an applied potential of 2.2 kV above the entrance potential of the IMS. The drift tube was operated at atmospheric pressure and room temperature (~700 torr and 21 °C in Pullman, WA). The dual gate IMS was pulsed from 5 to 8005 Hz for bradykinin and 5 to 2505 Hz for angiotensin II experiments. This difference in terminal frequency did not have any noticeable effects on the quality of the data collected but was changed to maximize experimental efficiency.

More detailed accounts of the atmospheric pressure, dual-gate PCB-IMS coupled to an ion trap mass spectrometer have been reported previously.[47,48] As seen in Figure S3, the full IMS includes the drift region and desolvation regions, which are equal in length. Consequently, the drift time measured from the FT-IMS experiment is approximately half of the total time the ions spend in the IMS. It is for this reason that when calculating the kinetics effects, the total drift time, estimated to be twice the time the ions take to traverse the drift region, is used. For a more in-depth conversation on the data analysis process used for the HDX kinetics, refer to our previous publication using amino acids.[31]

The countercurrent drift gas was N_2 at 2.5 L/min and modified using 99% pure methanol-OD (CH_3OD, (Cambridge Isotope Laboratories, Inc. (Andover, MA)) through the primary gas inlet at a variable flow rate between 5 and 300 μL/hr using a syringe pump. In these experiments, the drift time shifts after introducing the reactive vapor gas due to transient ion-neutral clustering.[41,46] To quantify the relative magnitude of the shift, the ratio K_i/K_o, is calculated where K_i is the mobility of the analytes with a user-defined concentration of modifier introduced into the drift gas, and K_o is the mobility of the analyte with no modifier. The degree of gHDX was deduced from the isotope window assuming pseudo-first-order kinetics and calculating the average *m/z* values for each analyte at each flow rate. This study assigned the isotope window by the number of exchangeable hydrogens. For example, bradykinin $[M+2H]^{+2}$ has 19 exchangeable hydrogens and was detected at *m/z* 530.7 (for a mass of 1061.4 Da). If all possible hydrogens are exchanged, the monoisotopic mass would be 1080.4 Da (or *m/z* 540.2). Under these conditions, the total isotopic window spans from *m/z* 530.7 to 540.2. For each replicate, the average *m/z* needed for kinetics analysis was calculated by a Gaussian fit of the isotope distribution within this range.

Simulation Setup and Conditions. A range of variables, including charge positioning and vapor molecule trajectory, contributed to the simulations aimed at capturing the distribution of vapor molecules bound to analyte ions and the specific analytes sites of vapor interaction. The partial charges on the three analyte ions (singly/doubly charged angiotensin II and doubly charged bradykinin) were determined via classical molecular dynamics (MD) simulation under vacuum conditions using the charge equilibrium method.[49] These QEq MD simulations were performed on the Large-scale Atomic/Molecular Massively Parallel Simulator, under the NVT ensemble, controlling ion temperature at 300 K by a Nose-Hoover thermostat.[50–52] The simulations were conducted for 10 ns with 0.25 fs time steps, during which the partial charges on each atom were exported at every 10000th time step (2.5 ps). The average partial charges were computed by averaging the charges from the period between 1 to 10 ns. The parameters for QEq, specifically the electronegativity and self-Coulombic interactions, were taken from Rappe and Goddard.[49] The additional hydrogen locations due to protonation were determined based on the highest two pKa value amino acids. The simulated protons were added to the two arginines for bradykinin ions, while for angiotensin II ions, they were placed on the arginine and the proline. We note that the proton location on angiotensin II has, at times, been reported to be at a different location from the proline. It was shown by Marchese *et al.* that the lowest energy protomer was protonated on the arginine and the histidine.[53] However, when moving the charge between residues, we found no significant impact on the recorded vapor-ion interactions when the excess hydrogen location was changed from proline to histidine.[54] This is detailed further in the supporting information in Figure S4. We, therefore, report results with excess charges placed on the arginine and proline.

Subsequently, the vapor trajectory-monitoring simulations about each of the three analyte ions were conducted using an in-house-developed code used previously in studying ion-ion recombination.[55] The ion under consideration was placed at the center of a cubical domain with one side length of 160.61 nm, with the cubic volume decided using the ideal gas law to represent near-atmospheric pressure and room temperature (750 torr and 300 K, respectively) with 10^5 nitrogen gas molecules. The methanol (MeOH) vapor molecules, as well as the 10^5 nitrogen (N_2) gas molecules, were randomly arranged in the cubical domain while avoiding overlap. The total number of MeOH molecules ranged from 10 to 100, representing experimental MeOH vapor pressure ranges of 0.075 to 0.75 torr, with the vapor pressure also calculated using the ideal gas model. We remark that simulations were performed assuming that MeOH and MeOD display similar behaviors with regard to ion-vapor clustering. The velocities for all atoms were initialized by sampling velocities from the Maxwell-Boltzmann distribution at the specified temperatures, and all-atom trajectories were iterated for 500 ns with a time step of 0.25 fs under the NVE ensemble. This was repeated at least 20 times, leading to a total simulation time of >10 μs for each vapor pressure and ion. The inter- and intra-molecular interactions were parameterized based on the general Amber force field, but the gas-gas interaction was neglected in this calculation, as done in previous gas-phase simulations.[55–58] The long-range Coulombic interaction was handled directly without the Ewald decomposition technique, as the system did not contain a net neutral charge. Furthermore, because the gas-vapor and vapor-vapor interactions occurred distally from the ion, these events do not significantly influence the simulated ion behavior or the nature of the vapor interaction with the ion surface. For these reasons, the vapor (MeOH) and gas (N_2) molecules were treated as interactionless point masses when their distances from the center ion were more than 10 nm (i.e., they moved ballistically at fixed velocity outside the 10 nm region, with their structures and potential effects only considered when within 10 nm of the ion). This coarse-grained approach is depicted schematically in Figure 1. This simplifying assumption substantially reduces computational cost but also neglects potential interactions beyond 10 nm radius, which, in select cases, may include the ion-methanol dipole potential outside this region. In preliminary simulations aimed at tuning this cut-off distance, we found increasing the radius had a negligible influence on results, suggesting that ion-dipole interactions need not be considered beyond 10 nm; however, Coulomb interactions, if present, are certainly significant beyond 10 nm .[57]

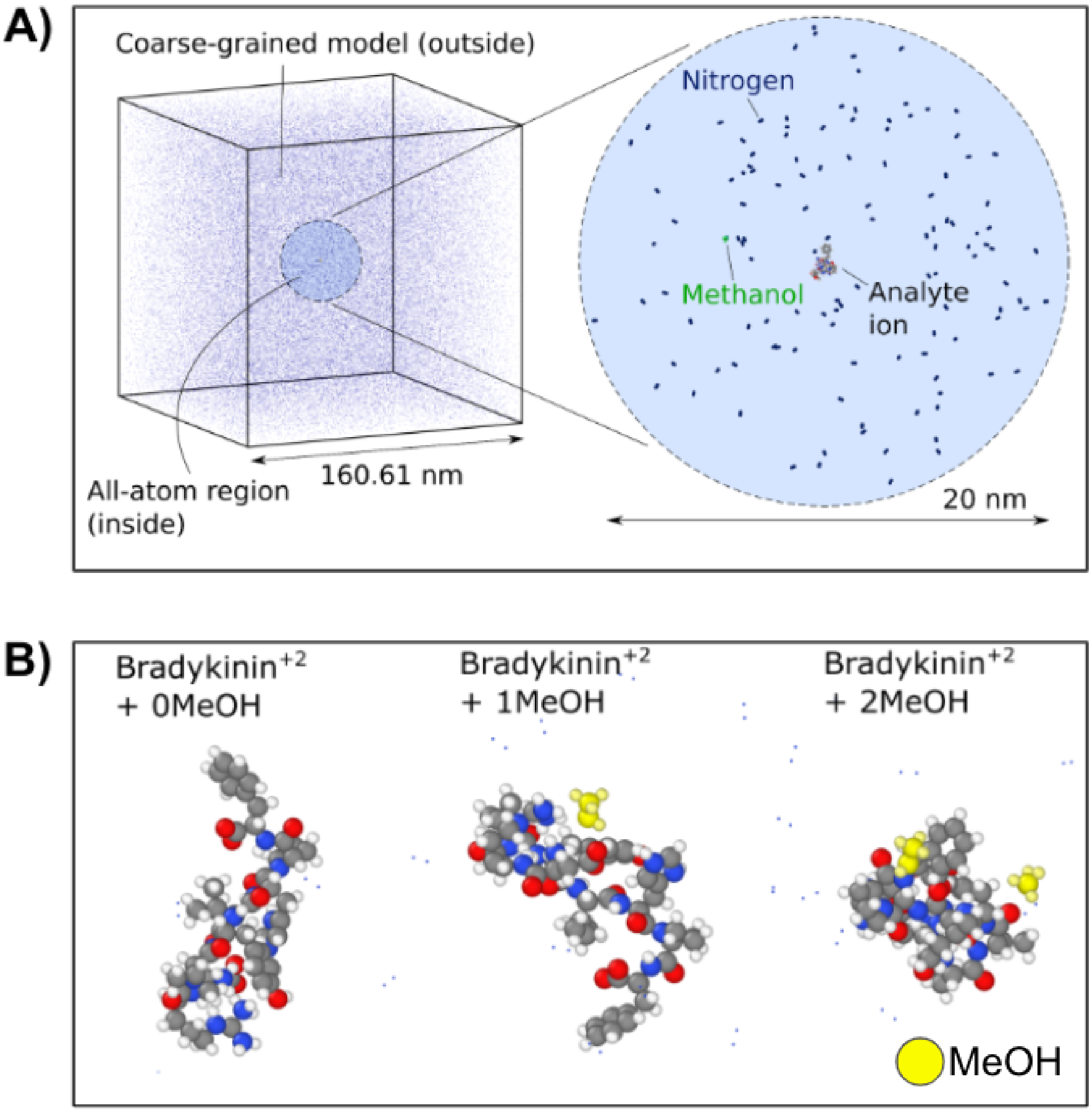

Figure 1. A) Depiction of the molecular dynamics simulations performed to examine MeOH clustering with angiotensin II and bradykinin ions. The left depicts the entire simulation domain, noting the cubical domain side length and depicting the inner sphere where potential interactions are considered. Outside the sphere, gas molecules and MeOH molecules drift ballistically. B) Snapshots of the molecular dynamics simulation with bradykinin. The methanol vapor is shown in yellow.

Periodic boundary conditions were applied on the domain walls, and periodically, the domain was recentered to the ion center-of-mass with distances traveled by the ion recorded for post-processing. Both pre-processing (QEq) and vapor molecule trajectory monitoring utilized velocity-

Verlet integration (unthermostatted, as noted above). In total, these simulations provided the coordinates and structures of each of the three ions and the coordinates of each of the vapor molecules relative to the ion.

Calculation of Gas-Phase Diffusion Coefficients. Post-processing first involved the estimation of ion mobilities and diffusion coefficients to compare the simulation results with the experimental ion mobility shifts caused by vapor molecule clustering. We remark because we utilize MD simulations to examine MeOH and ion interactions, calculations do not apply to fixed structures, as are commonly used when comparing ion mobility predictions to measurements. We instead calculated the diffusion coefficient from ion trajectories through two methods, and converted values to ion mobilities using the Sutherland-Einstein-Smoluchowski equation, assuming the low-field limit.[59] These methods naturally account for ion structure variability throughout simulations. The diffusion coefficient in MD simulations was computed using the Green-Kubo relation with the velocity auto-correlation function (VAF):

$$D_{VAF} = \frac{1}{3}\int_{0}^{\tau} < v(t) \cdot v(0) > dt$$

where the $v(t)$ is the ion center of mass velocity at time *t* and τ is the sampling time. The diffusion coefficient was also calculated via the mean square displacement (MSD):

$$D_{MSD} = \frac{1}{6\tau} < [r(\tau) - r(0)]_{\square}^{2} >$$

where $r(t)$ is the ion center of mass position at time equal *t*, and $[r(\tau) - r(0)]_{\square}^{2}$ represents square displacements. Importantly, by tracking the velocities and displacements of ion centers of mass, this method naturally accounts for vapor clustering effects on ion mobilities, as opposed to the calculation framework in our prior work, which hinges upon the estimation of the mobilities or diffusion coefficients as a function of an integer number of vapor molecules bound, as well as the fraction of time the ion spends with that integer number bound. In both diffusion coefficient calculations, the value τ needed to be large enough to approximate $\tau \rightarrow \infty$; we selected τ such that the VAF reaches <10^{-4} (normalized with initial correlation $v(0) \cdot v(0)$). Further details on calculations are provided in the supporting information.

Evaluation of Methanol Vapor Binding Properties. We remark that in simulations, MeOH clustering with other MeOH molecules, forming dimers, was rarely observed, and such dimers were short-lived. This is expected, as the MeOH number densities were far below saturation levels. MeOH monomers, therefore, collided with ions. To assess the level of MeOH clustering with each ion, post-processing was performed, which included calculating the number distribution of bound vapor molecules with the ion and the probability distribution of the vapor binding location on the ion. To determine the mean number of vapor molecules bound, we identified each vapor molecule in the simulation as in either the "binding" or "not binding" state based on its position and state in the previous time step. Initially, all vapor molecules were denoted as "not binding." Subsequently, at each time-step, we calculated the minimum distance between each vapor molecule and the ion (L_i) considering all atoms in the ion, using the equation:

$$L_i = \min_j \left\{ \left| r_j - r_i \right| \right\}_{j=1}^{N_{ion}}$$

where r_j is the position for each atom in the analyte ion, r_i is the center of mass of methanol molecule *i*, and N_{ion} is the number of atoms in the ion. When a vapor molecule was in the "not-binding" state in a prior time-step and L_i decreased below a prescribed arrival distance in the current time-step, L_a, the state for the vapor molecule in question was switched to "binding". Conversely, when for a vapor molecule in the "binding" state, if L_i became larger than a prescribed leaving distance, L_l, the state switched back to "not-binding." We set the arrival distance to 1 nm; this was empirically tuned to avoid grazing short-time encounters, while the leaving distance was set to a sufficiently large length of 10 nm to allow for rebound of vapor molecules back to the ion surface upon impingement. We remark that the results are only weakly sensitive to these choices provided the arrival distance is the 0.5-1.0 nm range and the leaving distance is larger than the arrival distance. The number of vapor molecules in the “binding” state was recorded every 10000 timesteps, which we used to construct the number distribution of vapor molecules bound, for variable vapor pressures. For the location probability, again every 10000 time-steps, for all vapor molecules in the “binding” state, the nearest exchangeable hydrogen was identified on the ion, assuming all hydrogens bonded with either nitrogen or oxygen were exchangeable, provided as Figure S1 and S2. We report location probabilities by amino acid in each ion. Subsequently, we use these values to construct cumulative location probabilities for fragment ions identified in CID experiments and compare these probabilities to the extent of HDX observed on each fragment ion.

Collision-Induced Dissociation Experiments. The fragmentation spectra for each species were collected both with and without the introduction of MeOD. Once the monoisotopic *m/z* was isolated, the normalized collision energy was increased until the precursor ion intensities were ~10% of the most intense fragment peak. From there, MeOD at 80 µL/hr was introduced, and the resulting spectra were collected under the same conditions.

A list of *b*- and *y*-type ion *m/z* values were generated for each amino acid sequence.[60] Only singly charged *m/z* fragment ions were used for $[M+H]^+$ angiotensin II, whereas both +1 and +2 charged ions were used for the $[M+2H]^{+2}$ species. These values were used to fit Gaussian distributions for each fragment ion mass if present in the MS/MS. If the fragment ion was detected in the CID spectra with no modifier present, then it was monitored upon the addition of MeOD. A Gaussian distribution was fit to the isotope profiles and used to calculate an average *m/z* for the ions. This is the value used to determine how many deuteriums were incorporated into the fragment on average.

For each amino acid in a given fragment's amino acid sequence, the probabilities of each amino acid interacting with a modifier were summed. Since the HDX occurs in the drift tube and the CID fragmentation occurs in the MS, the probabilities calculated for the intact protein are still representative of the probabilities of each residue in the fragment. This would not be true if the exchange had been done within the ion trap. However, we acknowledge that proton scrambling could mislead the HDX interpretation.[6,61,62] For that reason, we view these data qualitatively rather than attempting to parse though site-specific exchange data. Additional work using an alternative fragmentation method to limit deuteron scrambling will be done in the future.

Results and Discussion

Classic gHDX experiments illustrate the utility of ion reactions to constrain models of protein structure based on the rate of exchange and the percentage of deuterium uptake. Since our previous work suggests that the clustering equilibrium affects the exchange profiles observed, this experiment requires a few extra considerations.[31] It has been shown that the charge of an ion influences the ability of an ion to sequester vapors. For that reason, we will constrain our discussion to a comparison between the doubly charged species of angiotensin II and bradykinin for structural differences as they may affect HDX and clustering, and subsequently, discuss the effects of additional charges using two charge states of angiotensin II. Within the context of the present work, we expect angiotensin II to exchange faster and more completely than bradykinin, while the shifts in mobility due to transient clustering may look relatively similar for ions of the same charge state.

Structural Considerations of $[M+2H]^{+2}$ Ion: Bradykinin vs. Angiotensin II Our present work provides results from a different ionization compared to prior efforts. The Green and Wyttenbach reports use MALDI, which favors singly charged ions, whereas our work was done with ESI, which is known for creating a distribution of more highly charged species.[27,28] This explains why the singly charged species were more prevalent in the previous work. When using our spray conditions, the $[M+2H]^{+2}$ remained the dominant ion population. A peak around the correct *m/z* for the singly charged species could be seen sparingly, but after comparing mobility data of the two distributions, it was concluded to be doubly charged ions that had undergone charge reduction into the mass spectrometer.

Angiotensin II, however, formed the singly and doubly charged species under the same spray conditions. This peptide has also been studied using gHDX, where it was reported to exchange quite rapidly.[39] Angiotensin II has also been studied in the context of ion-neutral clustering with alcohols. Prior efforts by Rawat et al. reported shifts in angiotensin II mobility as a function of the increased vapor pressure of isopropyl alcohol and attributed this behavior to site-specific vapor uptake.[46] Within the context of the present work, we expected angiotensin II to exchange faster and more completely than bradykinin, while the shifts in mobility due to transient clustering may look relatively similar. The differences in gHDX rates for these analytes were attributed to elements of three-dimensional structural differences as discussed previously and, to a degree, reflected structure differences observed in the simulation.

The quantitative experimental results can be found in Table 2. The fast and slow rate constants come from the linear fits plotted using the *pwlf* 64 python package which also determines the breakpoint. The $H_{exchange}$ column comes from the greatest number of deuterium incorporated that cannot be attributed to a ^{13}C peak. Those numbers are divided by the number of theoretically exchangeable hydrogens to give the percentage in parentheses. The average total drift time is the average time the ions take to traverse the entire ion mobility cell (both the desolvation and drift region). This illustrates that the number of exchanges is not limited to the amount of time the ions spend in the presence of MeOD, but rather the difference in the analytes.

As seen in Figure 2, the nonlinear exchange profiles for the target peptide systems resemble the trends observed with K_i/K_o as reported previously with single amino acids.[31] For angiotensin II, the k_{fast} is twice that of bradykinin while k_{slow} is four times faster. Despite the differences in rate, the breakpoint and mobility shifts are quite similar, showing the significance of charge on the effect of clustering on rates. The total time the ions spend exposed to the modifier through the drift regions is also very similar, however, angiotensin II exchanges ⅔ of its exchangeable hydrogens, whereas bradykinin only exchanges ⅓. In summary, for the two ion distributions which are similar in *m/z* and mobility shifts, the fast rate, slow rate, and thus relative rates are unique to the analyte ion structure.

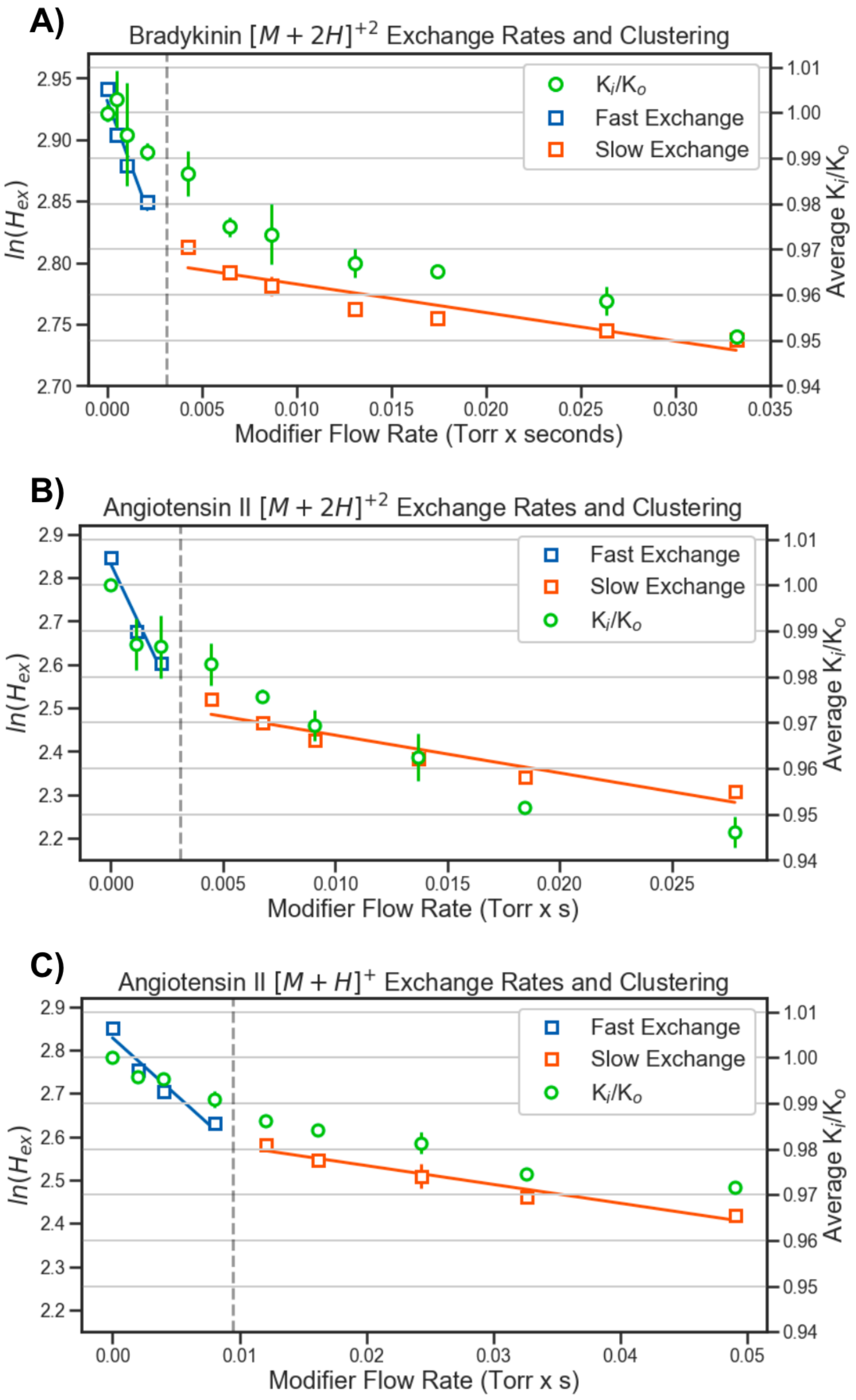

Figure 2(a-c). Pseudo-first order kinetics plots with shifts in mobility as a function of methanol-OD concentration for A) bradykinin $[M+2H]^{+2}$, B) angiotensin II $[M+2H]^{+2}$, and C) angiotensin II $[M+H]^{+}$. All of these analytes exhibit nonlinear trends in the kinetics data. For this reason, a fast rate (blue squares) and a slow rate (orange squares) are plotted with two linear fits. The highly correlated shifts in mobility quantified by the ratio K_i/K_0 are overlaid on the right y-axis and plotted in green circles. The error bars for all data are the standard deviation of three replicates at each flow rate with different electric fields.

The Role of Charge on Angiotensin II gHDX: $[M+2H]^{+2}$ vs. $[M+H]^{+}$ By comparing the exchange and shifts in mobility for two charge states of angiotensin II, the effects of added charge can be studied. The singly and doubly charged ions dominated the mass spectrum though conditions could be optimized to also observe the triply charged ions.

Since structural changes can arise when adding additional charge onto a peptide, the charge states with minimal differences in reported collisional cross sections would be better candidate analytes. In order to minimize the possible effects of structural changes induced by an additional proton, only the $[M+2H]^{+2}$ and $[M+H]^{+}$ ions will be compared which have only a 7% difference in CCS.[63] This way, the measured differences in gHDX and mobility shifts due to transient cluster formation will be more focused on the effects of additional charge.

As expected, the doubly charged species exchanges faster than the singly charged species; the $[M+2H]^{+2}$ ions' k_{fast} is four times faster and k_{slow} is twice as fast than the $[M+H]^{+}$ ions. Interestingly, the relative rate and mobility changes for the singly charged species are nearly half that of the doubly charged species, further supporting that gHDX rates are influenced by clustering. The higher charge states attract more vapor modifiers than lower charge states and thus have faster initial rates but a larger reduction in rate as the modifier vapor concentration is increased, pushing equilibria toward clusters. To elaborate further on this point, the faster initial rate is due to the increased collision frequency for the doubly charged ions inducing more cluster formation as the partial pressure of the modifier is increased. Clusters sterically hinder further access to the exchange site which results in a drop in rate that is more pronounced for the doubly charged species.

The breakpoints are different for each charge state, however, the average K_i/K_0 of the flows bracketing the breakpoint is 0.985 $[M+2H]^{+2}$ and 0.989 for $[M+H]^{+}$. These data support that clustering slows down the rate of exchange and could be a cause of the nonlinear behavior thus controlling where the breakpoint is calculated. It is also important to note that the extent of deuterium incorporation is greater for the doubly charged species despite spending roughly half the time within the drift tube, highlighting that the data recorded differs on the basis of gas phase reactivity rather than kinetic limitations.

Analyte	k_{fast}	k_{slow}	k_{fast}/k_{slow}	**Breakpoint (Torr x sec)**	$H_{exchanges}$	**Avg. Total t_{drift} (ms)**	**% K_0 change**
Bradykinin^{+2}	6.55E-12	3.45E-13	19.0	0.0031	6 (32%)	31	4.9%
Angiotensin II^{+2}	1.62E-11	1.29E-12	12.6	0.0031	12 (67%)	32	5.4%
Angiotensin II^{+}	3.92E-12	6.48E-13	6.0	0.0095	8 (47%)	57	2.8%

Table 2: gHDX IM-MS Experimental Results.

Mobility Shift Simulations. Videos of MeOH clustering about Bradykinin^{+2} and Angiotensin II^{+2} for a MeOH vapor pressure of 1.5 Torr are provided as supporting information. Snapshot images of one and two MeOH molecules bound in simulations are also provided. From simulations, the ion mobilities computed using both the VAF and MSD approaches were normalized by the mobility value K_0, which was obtained from MD simulations conducted in the absence of MeOH vapor. Figure 3 displays a comparison of the normalized mobilities from MD trajectory calculations in comparison to experimental results for three different analyte ions. Overall, the ion mobilities computed from both the VAF and MSD methods agreed well, indicating that the sampling (or total calculation time) of the MD simulation was sufficient to monitor ion diffusion. The trend of mobility reduction with increasing vapor pressure was also observed in the MD simulations. However, distinct from experimental measurements, we observed no discernable decreases in mobilities for the lowest vapor pressures examined, with mobilities fluctuating for vapor pressures below 1.0 Torr. Nonetheless, the magnitude of the mobility shifts observed experimentally and in simulations are comparable, only with slightly higher vapor pressures required to cause shifts similar to those observed experimentally. We remark that in comparing measured and calculated mobility in polyatomic gasses, it is frequently necessary to tune potential interactions or to introduce diffuse scattering models (when “frozen” ions are modeled) in order to bring calculations in line with measurements.[65–69] Modifying potential interactions, including parameter tuning, varying the partial charge optimization method, or using alternative potential functions, may also help to resolve the small mobility shift difference between simulation and experiment here. However, even without these modifications, our results suggest that simulations do capture the approximate number distributions of binding vapor molecules leading to observed mobility shifts; hence they have value in examining vapor binding number distributions and binding location probabilities.

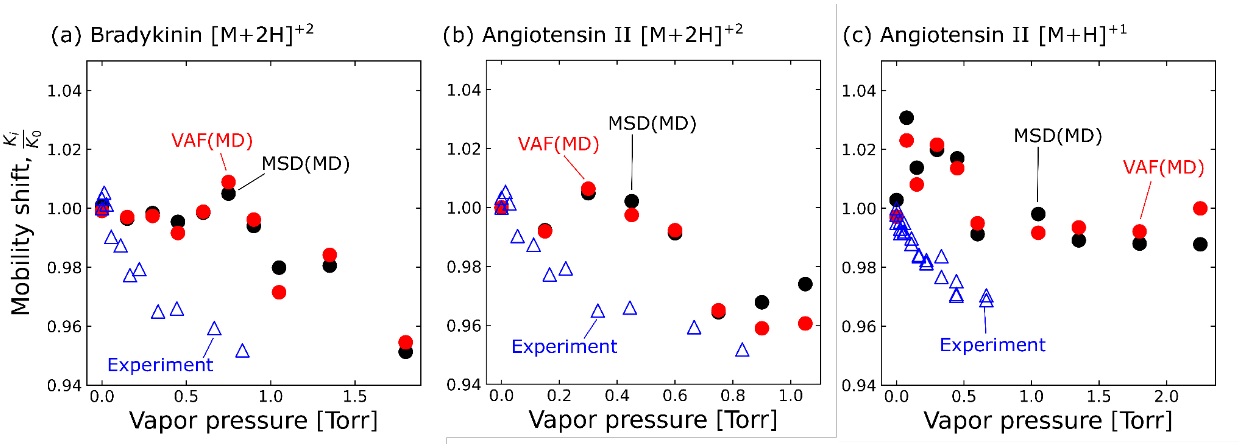

Figure 3. The mobility shifts of three analytes, bradykinin [M+2H]$^{+2}$ (a), Angiotensin II [M+2H]$^{+2}$ (b), and Angiotensin II [M+H]$^{+1}$ (c) observed in the experiment (blue triangle) and predicted based on the diffusion coefficient calculation with two different ways in the MD simulation (VAF: red circle and MSD: black circle).

Canonical Vapor Binding Distributions. The average number of MeOH vapor molecules adsorbed onto the analyte surface, denoted as N, was calculated by monitoring the quantity of MeOH molecules marked as "binding" at any given instant throughout the simulation duration and subsequently computing the mean value, represented as $\overline{N}$. Figure 4 depicts $\overline{N}$ as a function of

MeOH vapor pressure for each analyte, displaying higher values for angiotensin II^{+2} than angiotensin II^{+1}, with bradykinin positioned between the two angiotensin II species. The prevailing trend observed for $\bar{N}$ is that an elevated vapor pressure results in more binding vapor molecules for each of the three analytes. This can first be simply attributed to the increased frequency of vapor molecule collisions with ions at higher vapor pressures or, in other words, at augmented vapor concentrations. Figure S5 substantiates this observation, illustrating the linear relationship between the vapor collision frequency and MeOH vapor pressure. The collision frequency was derived by counting the instances when vapor labels switched from "non-binding" to "binding." The corresponding collision frequency slopes for bradykinin^{+2}, angiotensin II^{+2}, and angiotensin II^{+1} were 0.195, 0.208, and 0.093 ns^{-1} torr^{-1}, respectively. We also find that the collision frequency is predominantly governed by the long-range force between the "net charge" of the analyte ion and the dipole of the vapor (i.e., the ion-dipole interaction). For this reason, the collision frequency slope of angiotensin II^{+2} is larger than that of singly charged angiotensin II. However, the collision frequency slopes of angiotensin II^{+2} and bradykinin^{+2} are similar values, also indicating that short-range forces and minor structural deviations affect the collision frequency to only a minor extent. Revisiting the comparison of $\bar{N}$ for different analytes displayed in Figure 4, despite having similar collision frequencies, bradykinin^{+2} and angiotensin II^{+2} do have disparate $\bar{N}$ values. This suggests that the governing physical properties determining the binding duration (the time difference between the vapor's arrival and leaving times) are not only determined by the net charge but also depend upon local properties, including short-range interactions or partial charge levels.

Also of interest is the distribution of vapor molecules bound for each ion at variable vapor pressure; we plot these distributions in Figure 5 for bradykinin^{+2} and in Figures S6 and S7 for angiotensin II^{+1} and angiotensin II^{+2}, respectively. In addition to distributions extracted directly from simulations, we also plot Poisson distributions using $\bar{N}$ as the mean value. Overall, we find strong agreement at all vapor pressures for each of the three analytes between the directly-calculated distributions and Poisson distributions. Deviations evident for larger numbers of vapor molecules bound are attributable to plotting results on a logarithmic scale, amplifying these differences, and to increasing variability in simulation results due to poorer counting statistics for low probability N values. Therefore, in spite of binding influenced by ion and vapor molecule properties and local structures, we find that the distribution of vapor molecules bound for subsaturated, equilibrated conditions can be approximated by a rather simple Poisson distribution, only requiring an estimate of the mean number of vapor molecules bound, $\bar{N}$. The extent to which this conclusion is generalizable, however, would need to be addressed in future work, as it is certainly possible that for particular ion-vapor molecule combinations, a specific number of vapor molecules bound may be anomalously probable (i.e., a so-called magic number cluster) or improbable (an anti-magic cluster), which is not captured by Poisson statistics.

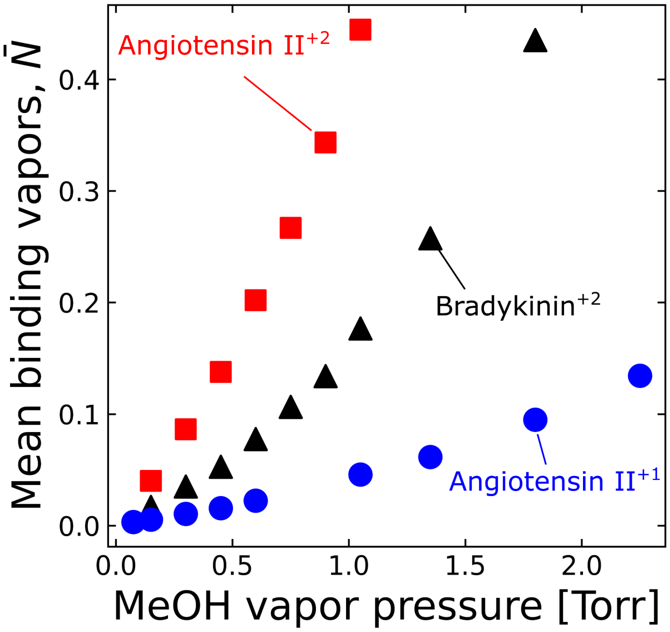

Figure 4. Mean binding vapors, N, as a function of MeOH vapor pressure in different analytes. The black triangle is doubly charged bradykinin, the red square is doubly charged angiotensin II, and the blue circle is doubly charged angiotensin II.

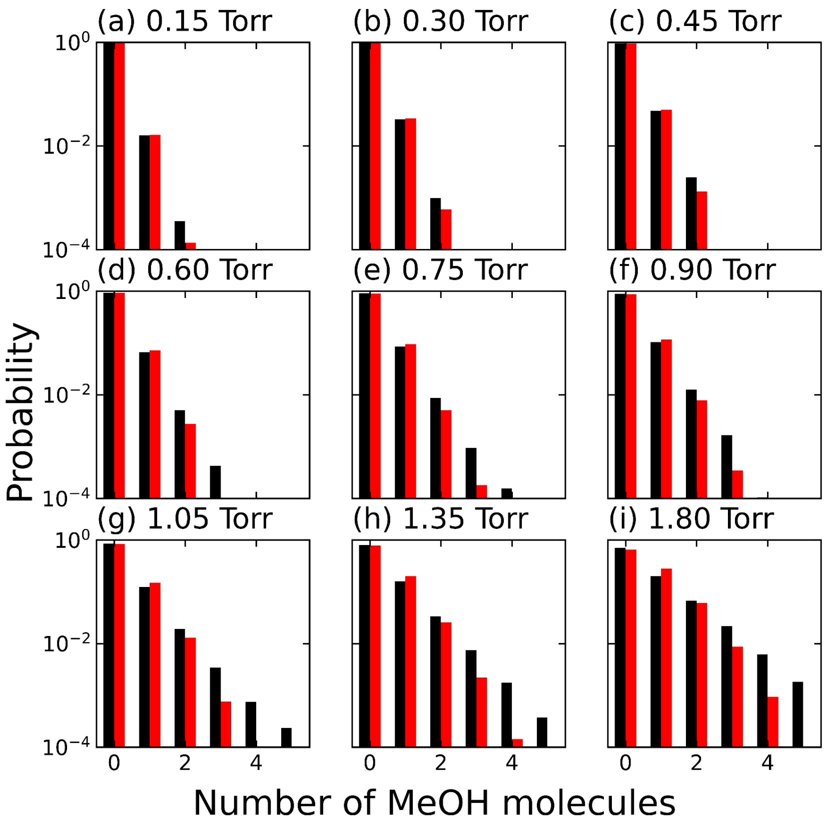

Figure 5. MeOH vapor binding distributions on the doubly charged bradykinin. Black and red bars respectively indicate results from MD vapor trajectory calculation and prediction with the Poisson distribution.

Localized Vapor Binding Distributions. To better understand MeOH dynamics upon binding, local MeOH vapor binding probabilities were calculated for each amino acid with an exchangeable hydrogen in doubly charged bradykinin across a range of vapor pressures, with results displayed in Figure 6. Similar calculations were performed for doubly and singly charged angiotensin II, with results available in the Supporting Information, Figures S8 and S9, respectively. Notably, the hydrogen exchangeable sites in bradykinin are limited to four amino acids: serine and the two terminal arginine residues, as depicted in Figure S2, as well as the amide backbone hydrogens. Interestingly, the proline residues, which have no exchangeable hydrogens either from side chains or the amide backbone, result in local binding probabilities consistently at zero. The Gly^{4} residue also has a consistent zero binding probability despite one local exchangeable amide hydrogen which could be protected from the solvent by the adjacent prolines. In contrast, the phenylalanine residues have exchangeable amide hydrogens and a nonzero probability of vapor binding.

We observe that the local vapor binding probability distributions are rather insensitive to vapor pressure, suggesting that vapor binding is predominantly governed by one-to-one interactions between the vapor molecule and analyte and expected for vapor binding probability distributions where multiple vapor molecules simultaneously bound is rare. The two terminal arginine sites (Arg^1 and Arg^9) show the highest probabilities, whereas the central phenylalanine site (Phe^5) shows the lowest nonzero probability. This concave-down distribution pattern is also observed in the two angiotensin II ions (though weaker for the doubly charged angiotensin II ion). This suggests that the accessibility of MeOH vapor to the more central amino acid residues is hindered due to interference from surrounding amino acids, or, in the case of bradykinin, preference for terminal charge sites, leading to higher binding probability at the terminal sites. Such binding patterns are common in collision-limited systems in the gas phase; for example, diffusion-limited aggregate structures form frequently in gas phase collision-limited processes due to limited accessibility to structural interiors in colliding partners. It is not surprising that this finding qualitatively extends to chain-like ions.

We also calculated the partial charges and MeOH vapor accessible surface areas (ASA) for each amino acid comprising the analytes. The local binding probabilities are plotted against these two properties in Figure 7, with details of the calculation procedures for these parameters in the Supporting Information. To quantify the correlation between the local binding probability and these two properties (partial charges and ASA), Pearson's correlation coefficients were found to be -0.079 and 0.340 for partial charges and ASA, respectively. These results suggest that the correlation between the local binding probability and partial charges is negligible, while a weak correlation is present with the ASA. Local binding, therefore, appears to be predominantly driven by the structural characteristics of the ions examined.

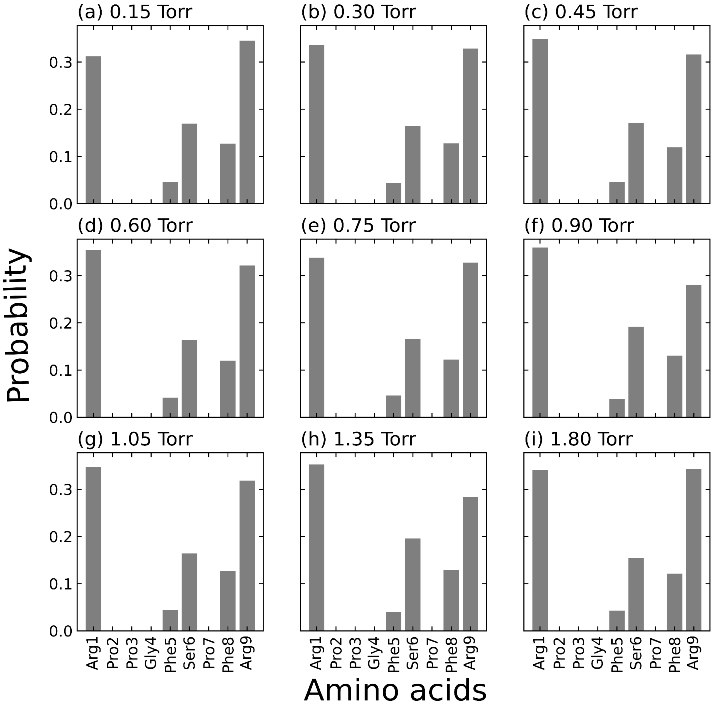

Figure 6. The binding location probability distribution on each amino acid of doubly charged bradykinin, Arg1, Pro2, Pro3, Gly4, Phe5, Ser6, Pro7, Phe8, and Arg9. (a) to (i) represent different vapor pressures, 0.15 to 1.80 Torr.

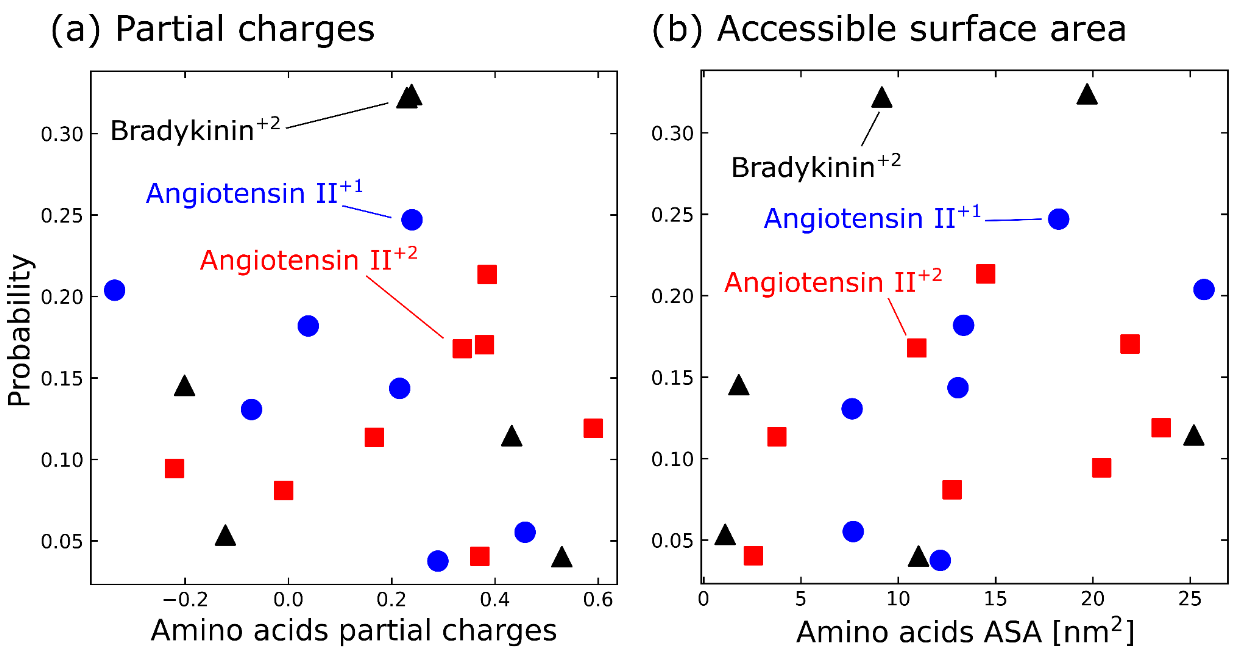

Figure 7. Binding location probability to each amino acid versus amino acid partial charges (a) and versus amino acid accessible surface area (ASA). The black triangle corresponds to the doubly charged bradykinin, the red square represents doubly charged angiotensin II, and the blue circle is the doubly charged angiotensin II.

The Role of Accessible Surface Area, Clustering, and gHDX. The weak correlation between ion-neutral clustering and accessible surface area of each residue observed in MD simulations has been a topic of debate in gHDX literature for biological molecules.[28,70] Robinson and Williams paired FAIMS-derived CCS values with gHDX extent and found that, while gHDX was sensitive to conformational changes, the changes were not correlated with the CCS values.[70] However, MD simulations of the gHDX experiment with bradykinin concluded that the surface availability of basic sites and their respective distances impacted the calculated rate.[28] While ASA cannot be ignored in gHDX and, as shown in this work, ion-neutral clustering, a clear distinction needs to be made. Vapor-ion interactions are necessary for a reaction to proceed but do not necessarily ensure a reaction (e.g., gHDX) will occur. Stated differently, the local environment of a solvent-accessible hydrogen (e.g., hydrogen-bonded) may still preclude the possibility of gHDX. In fact, this behavior has been exploited in prior efforts as a control condition when probing gas-phase clustering and HDX.[31] When combined with MD, the present set of experiments aids in the placement of constraints when balancing the degree of solvent accessibility with the observed rates of HDX.

Collision-Induced Dissociation of Exchanged Peptides. Trends in collision-induced dissociation (CID) spectra with and without the modifier present were evaluated. A list of fragment ions detected and how many hydrogens each exchanged can be found in Figure S10. While more fragment ions were observed for bradykinin, the overall intensity of the fragment ions was much lower than with angiotensin II. Interestingly, the trends observed with the intact peptide gHDX match interpretations from the CID data; doubly charged angiotensin II exchanges more than doubly charged bradykinin and singly charged angiotensin II. Since CID occurs on time scales that allow for scrambling, we use these data to qualitatively compare experimental and simulated data. Questions related to the degree of HDX realized per residue will be the focus of future work using faster fragmentation methods (e.g., UVPD).[71,72]

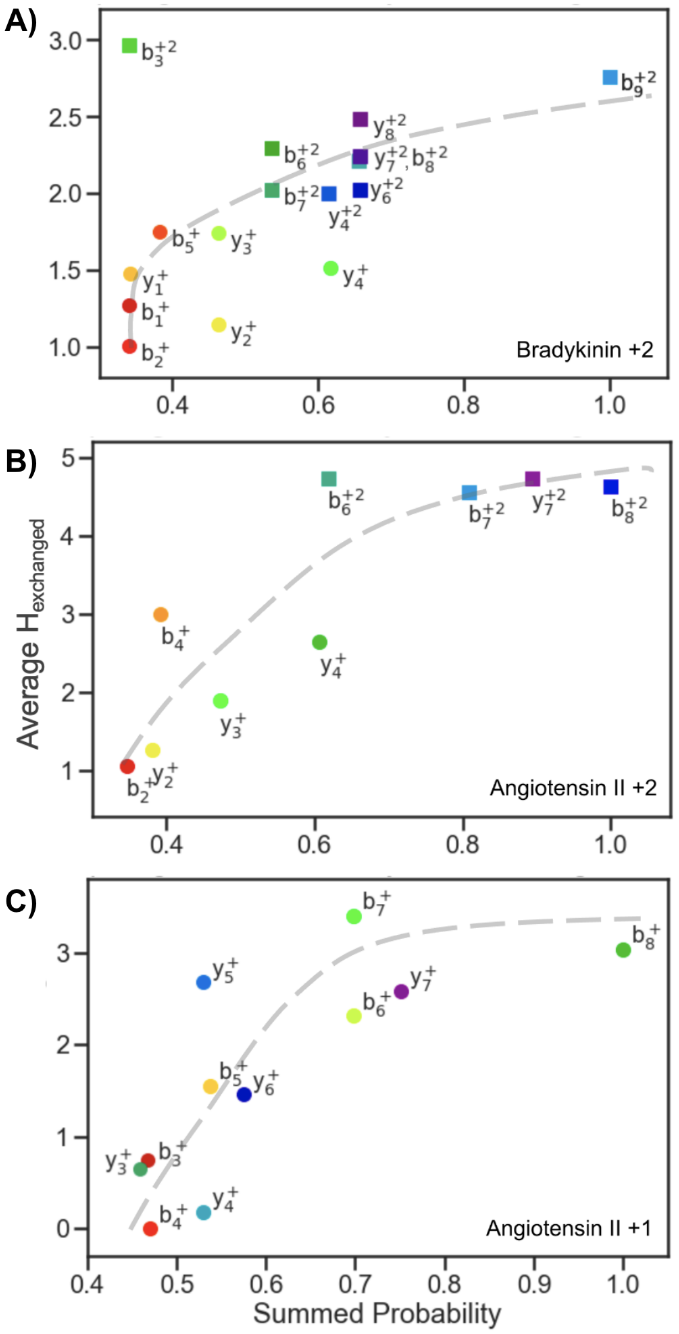

Figure 8 (A-C). CID HDX versus probability of the fragment ion to form a cluster for A) bradykinin^{+2}, B) angiotensin II^{+2}, and C) angiotensin II^{+}. The summed probability is calculated by adding the probability of each amino acid forming a cluster from the MD simulation. The dashed line only serves to guide the eye to the observed trends.

Correlating Clustering Probability and Peptide Fragment gHDX. The average number of exchanged hydrogens was plotted versus the per residue summed probability. Generally, as the summed probability increases for a fragment ion, the average number of exchanges also increases. This trend is seen clearly in **Figure 8 A)** and **B)** for angiotensin II $[M+H]^+$ and $[M+2H]^{+2}$, respectively. While the average $H_{exchanged}$ increases with probability for bradykinin as well, there are a few outliers, particularly the doubly charged b_3 ion, RPP. The other outliers are the singly charged y_2 and y_4 ions to form FR and SPFR, which exchange less than the trend. It could be theorized that these ions originate from a peptide with a charge on the C-terminus arginine involved in some form of three-dimensional structure and is thus not accessible by the deuterated vapor for exchange.

Conclusions

The most encouraging aspect of these data is that the complex equilibria of peptide ion-neutral interactions, examined from two independent perspectives on a per-residue basis, gHDX experiments, and simulated cluster formation, are directly related. This suggests that these two methods can be used to provide complementary information about these interactions. These independent observations contribute to the notion that ion-vapor clustering greatly mediates gHDX. Similar conclusions have been drawn throughout the gHDX literature with regard to the relay mechanism that is shown to proceed through a “long-lived ion-neutral complex” involving two hydrogen bonds.[25] By combining those results with the ones presented here, one can imagine the nature of these reactions as the ions traverse the drift tube: ions move through the neutral gas, mostly nitrogen, but when a MeOD interacts with the peptide, it can sample the accessible surface area forming a cluster. When, or if, the vapor reaches a residue that can form the double hydrogen bonds necessary for exchange through the relay mechanism, gHDX can proceed. Our study provides evidence that the exchange could take place while the ion is locally solvated.

Although this concept may appear intuitive, performing these reactions within an instrument incapable of quantifying changes in the complex equilibria that exist between ions and the reactive modifier, such as a trapping mass spectrometer, could not quantify both the HDX reactivity cluster formation.[1,13,25,73,74] For this reason, studying clustering (and subsequent gHDX) within an IMS enables data for both phenomena to be recorded in a single experiment and provides information past *m/z*. Expansion on this work could be useful in deducing protein structural differences, post-translational modifications, and selecting the most native-like charge states.

Conflicts of Interest

The authors declare no conflict of interest.

Supporting Information

The primary document of Supporting Information contains additional details regarding the instrumental configuration, methods of simulation, and associated results for the tandem MS experiments of selected ion.

Bradykinin movie: clip of a bradykinin ion clustering with MeOH in the presence of N_2

Angiotensin II movie: clip of an angiotensin II ion clustering with MeOH in the presence of N_2

Acknowledgments

The contributions by C. Hogan and T. Tamadate were supported by US NSF 2002852. H. Schramm and B. Clowers acknowledge the support provided by US NSF 2003042.

References

(1) Chaturvedi, R.; Webb, I. K. Multiplexed Conformationally Selective, Localized Gas-Phase Hydrogen Deuterium Exchange of Protein Ions Enabled by Transmission-Mode Electron Capture Dissociation. *Anal. Chem.* **2022**, *94* (25), 8975–8982.
(2) Tsybin, Y. O.; Haselmann, K. F.; Emmett, M. R.; Hendrickson, C. L.; Marshall, A. G. Charge Location Directs Electron Capture Dissociation of Peptide Dications. *J. Am. Soc. Mass Spectrom.* **2006**, *17* (12), 1704–1711.
(3) Horn, D. M.; Breuker, K.; Frank, A. J.; McLafferty, F. W. Kinetic Intermediates in the Folding of Gaseous Protein Ions Characterized by Electron Capture Dissociation Mass Spectrometry. *J. Am. Chem. Soc.* **2001**, *123* (40), 9792–9799.
(4) Morrison, L. J.; Brodbelt, J. S. Charge Site Assignment in Native Proteins by Ultraviolet Photodissociation (UVPD) Mass Spectrometry. *Analyst* **2016**, *141* (1), 166–176.
(5) Morrison, K. A.; Clowers, B. H. Differential Fragmentation of Mobility-Selected Glycans via Ultraviolet Photodissociation and Ion Mobility-Mass Spectrometry. *J. Am. Soc. Mass Spectrom.* **2017**, *28* (6), 1236–1241.
(6) Wysocki, V. H.; Tsaprailis, G.; Smith, L. L.; Breci, L. A. Mobile and Localized Protons: A Framework for Understanding Peptide Dissociation. *J. Mass Spectrom.* **2000**, *35* (12), 1399–1406.
(7) Young, M. N.; Bleiholder, C. Molecular Structures and Momentum Transfer Cross Sections: The Influence of the Analyte Charge Distribution. *J. Am. Soc. Mass Spectrom.* **2017**, *28* (4), 619–627.
(8) Schnier, P. D.; Gross, D. S.; Williams, E. R. On the Maximum Charge State and Proton Transfer Reactivity of Peptide and Protein Ions Formed by Electrospray Ionization. *J. Am. Soc. Mass Spectrom.* **1995**, *6* (11), 1086–1097.
(9) Valentine, S. J.; Counterman, A. E.; Clemmer, D. E. Conformer-Dependent Proton-Transfer Reactions of Ubiquitin Ions. *J. Am. Soc. Mass Spectrom.* **1997**, *8* (9), 954–961.
(10) Pitteri, S. J.; McLuckey, S. A. Recent Developments in the Ion/ion Chemistry of High-Mass Multiply Charged Ions. *Mass Spectrom. Rev.* **2005**, *24* (6), 931–958.
(11) Foreman, D. J.; McLuckey, S. A. Recent Developments in Gas-Phase Ion/Ion Reactions for Analytical Mass Spectrometry. *Anal. Chem.* **2020**, *92* (1), 252–266.
(12) Hill, H. H.; Hill, C. H.; Asbury, G. R.; Wu, C.; Matz, L. M.; Ichiye, T. Charge Location on Gas Phase Peptides. *Int. J. Mass Spectrom.* **2002**, *219* (1), 23–37.
(13) Suckau, D.; Shi, Y.; Beu, S. C.; Senko, M. W.; Quinn, J. P.; Wampler, F. M., 3rd; McLafferty, F. W. Coexisting Stable Conformations of Gaseous Protein Ions. *Proc. Natl. Acad. Sci. U. S. A.* **1993**, *90* (3), 790–793.
(14) Valentine, S. J.; Clemmer, D. E. H/D Exchange Levels of Shape-Resolved Cytochrome c Conformers in the Gas Phase. *J. Am. Chem. Soc.* **1997**, *119* (15), 3558–3566.
(15) Lifshitz, C. A Review of Gas-Phase H/D Exchange Experiments: The Protonated Arginine Dimer and Bradykinin Nonapeptide Systems. *Int. J. Mass Spectrom.* **2004**, *234* (1), 63–70.
(16) Campbell, S.; Rodgers, M. T.; Marzluff, E. M.; Beauchamp, J. L. Structural and Energetic Constraints on Gas Phase Hydrogen/deuterium Exchange Reactions of Protonated Peptides with D2O, CD3OD, CD3CO2D, and ND3. *J. Am. Chem. Soc.* **1994**, *116* (21), 9765–9766.
(17) Khakinejad, M.; Kondalaji, S. G.; Maleki, H.; Arndt, J. R.; Donohoe, G. C.; Valentine, S. J. Combining Ion Mobility Spectrometry with Hydrogen-Deuterium Exchange and Top-down MS for Peptide Ion Structure Analysis. *J. Am. Soc. Mass Spectrom.* **2014**, *25* (12), 2103–2115.
(18) Chen, X.; Yu, L.; Steill, J. D.; Oomens, J.; Polfer, N. C. Effect of Peptide Fragment Size on the Propensity of Cyclization in Collision-Induced Dissociation: Oligoglycine b(2)-b(8). *J.*

Am. Chem. Soc. **2009**, *131* (51), 18272–18282.

(19) Rand, K. D.; Pringle, S. D.; Murphy, J. P., 3rd; Fadgen, K. E.; Brown, J.; Engen, J. R. Gas-Phase Hydrogen/deuterium Exchange in a Traveling Wave Ion Guide for the Examination of Protein Conformations. *Anal. Chem.* **2009**, *81* (24), 10019–10028.

(20) Pan, J.; Heath, B. L.; Jockusch, R. A.; Konermann, L. Structural Interrogation of Electrosprayed Peptide Ions by Gas-Phase H/D Exchange and Electron Capture Dissociation Mass Spectrometry. *Anal. Chem.* **2012**, *84* (1), 373–378.

(21) Carrascosa, E.; Pellegrinelli, R. P.; Rizzo, T. R.; Muyskens, M. A. Cryogenic Infrared Action Spectroscopy Fingerprints the Hydrogen Bonding Network in Gas-Phase Coumarin Cations. *J. Phys. Chem. A* **2020**, *124* (48), 9942–9950.

(22) Warnke, S.; Ben Faleh, A.; Pellegrinelli, R. P.; Yalovenko, N.; Rizzo, T. R. Combining Ultra-High Resolution Ion Mobility Spectrometry with Cryogenic IR Spectroscopy for the Study of Biomolecular Ions. *Faraday Discuss.* **2019**, *217* (0), 114–125.

(23) Jurneczko, E.; Barran, P. E. How Useful Is Ion Mobility Mass Spectrometry for Structural Biology? The Relationship between Protein Crystal Structures and Their Collision Cross Sections in the Gas Phase. *Analyst* **2011**, *136* (1), 20–28.

(24) Cassady, C. J.; Carr, S. R. Elucidation of Isomeric Structures for Ubiquitin [M + 12H]12+ Ions Produced by Electrospray Ionization Mass Spectrometry. *J. Mass Spectrom.* **1996**, *31* (3), 247–254.

(25) Campbell, S.; Rodgers, M. T.; Marzluff, E. M.; Beauchamp, J. L. Deuterium Exchange Reactions as a Probe of Biomolecule Structure. Fundamental Studies of Gas Phase H/D Exchange Reactions of Protonated Glycine Oligomers with D2O, CD3OD, CD3CO2D, and ND3. *J. Am. Chem. Soc.* **1995**, *117* (51), 12840–12854.

(26) Gard, E.; Willard, D.; Bregar, J.; Green, M. K.; Lebrilla, C. B. Site Specificity in the H-D Exchange Reactions of Gas-Phase Protonated Amino Acids with CH3OD. *J. Mass Spectrom.* **1993**, *28* (12), 1632–1639.

(27) Green, M. K.; Lebrilla, C. B. The Role of Proton-Bridged Intermediates in Promoting Hydrogen-Deuterium Exchange in Gas-Phase Protonated Diamines, Peptides and Proteins. *Int. J. Mass Spectrom. Ion Process.* **1998**, *175* (1), 15–26.

(28) Wyttenbach, T.; Bowers, M. T. Gas Phase Conformations of Biological Molecules: The Hydrogen/deuterium Exchange Mechanism. *J. Am. Soc. Mass Spectrom.* **1999**, *10* (1), 9–14.

(29) Freitas, M. A.; Hendrickson, C. L.; Emmett, M. R.; Marshall, A. G. Gas-Phase Bovine Ubiquitin Cation Conformations Resolved by Gas-Phase Hydrogen/deuterium Exchange Rate and extent11Dedicated to Professor Michael T. Bowers on the Occasion of His 60th Birthday. *Int. J. Mass Spectrom.* **1999**, *185-187*, 565–575.

(30) Wyttenbach, T.; Bleiholder, C.; Bowers, M. T. Factors Contributing to the Collision Cross Section of Polyatomic Ions in the Kilodalton to Gigadalton Range: Application to Ion Mobility Measurements. *Anal. Chem.* **2013**, *85* (4), 2191–2199.

(31) Schramm, H. M.; Tamadate, T.; Hogan, C. J.; Clowers, B. H. Ion-Neutral Clustering Alters Gas-Phase Hydrogen-Deuterium Exchange Rates. *Phys. Chem. Chem. Phys.* **2023**. https://doi.org/10.1039/d2cp04388b.

(32) Valentine, S. J.; Clemmer, D. E. Temperature-Dependent H/D Exchange of Compact and Elongated Cytochrome c Ions in the Gas Phase. *J. Am. Soc. Mass Spectrom.* **2002**, *13* (5), 506–517.

33) Gabelica, V.; Shvartsburg, A. A.; Afonso, C.; Barran, P.; Benesch, J. L. P.; Bleiholder, C.; Bowers, M. T.; Bilbao, A.; Bush, M. F.; Campbell, J. L.; *et al.* Recommendations for Reporting Ion Mobility Mass Spectrometry Measurements. *Mass Spectrom. Rev.* **2019**, *38* (3), 291–320.

(34) Donohoe, G. C.; Khakinejad, M.; Valentine, S. J. Ion Mobility Spectrometry-Hydrogen Deuterium Exchange Mass Spectrometry of Anions: Part 1. Peptides to Proteins. *J. Am.*

Soc. Mass Spectrom. **2015**, *26* (4), 564–576.

(35) Karanji, A. K.; Khakinejad, M.; Kondalaji, S. G.; Majuta, S. N.; Attanayake, K.; Valentine, S. J. Comparison of Peptide Ion Conformers Arising from Non-Helical and Helical Peptides Using Ion Mobility Spectrometry and Gas-Phase Hydrogen/deuterium Exchange. *J. Am. Soc. Mass Spectrom.* **2018**, *29* (12), 2402–2412.

(36) Maleki, H.; Maurer, M. M.; Ronaghi, N.; Valentine, S. J. Ion Mobility, Hydrogen/Deuterium Exchange, and Isotope Scrambling: Tools to Aid Compound Identification in 'Omics Mixtures. *Anal. Chem.* **2017**, *89* (12), 6399–6407.

(37) Khakinejad, M.; Ghassabi Kondalaji, S.; Tafreshian, A.; Valentine, S. J. Comprehensive Gas-Phase Peptide Ion Structure Studies Using Ion Mobility Techniques: Part 2. Gas-Phase Hydrogen/Deuterium Exchange for Ion Population Estimation. *J. Am. Soc. Mass Spectrom.* **2017**, *28* (5), 960–970.

(38) Maleki, H.; Karanji, A. K.; Majuta, S.; Maurer, M. M.; Valentine, S. J. Ion Mobility Spectrometry-Mass Spectrometry Coupled with Gas-Phase Hydrogen/Deuterium Exchange for Metabolomics Analyses. *J. Am. Soc. Mass Spectrom.* **2018**, *29* (2), 230–241.

(39) Freitas, M. A.; Hendrickson, C. L.; Emmett, M. R.; Marshall, A. G. High-Field Fourier Transform Ion Cyclotron Resonance Mass Spectrometry for Simultaneous Trapping and Gas-Phase Hydrogen/deuterium Exchange of Peptide Ions. *J. Am. Soc. Mass Spectrom.* **1998**, *9* (10), 1012–1019.

(40) Levy-Seri, E.; Koster, G.; Kogan, A.; Gutman, K.; Reuben, B. G.; Lifshitz, C. An Electrospray Ionization−Flow Tube Study of H/D Exchange in Protonated Bradykinin. *J. Phys. Chem. A* **2001**, *105* (23), 5552–5559.

(41) Kwantwi-Barima, P.; Ouyang, H.; Hogan, C. J., Jr; Clowers, B. H. Tuning Mobility Separation Factors of Chemical Warfare Agent Degradation Products via Selective Ion-Neutral Clustering. *Anal. Chem.* **2017**, *89* (22), 12416–12424.

(42) Kwantwi-Barima, P.; Hogan, C. J., Jr; Clowers, B. H. Deducing Proton-Bound Heterodimer Association Energies from Shifts in Ion Mobility Arrival Time Distributions. *J. Phys. Chem. A* **2019**, *123* (13), 2957–2965.

(43) Ieritano, C.; Rickert, D.; Featherstone, J.; Honek, J. F.; Campbell, J. L.; Blanc, J. C. Y. L.; Schneider, B. B.; Hopkins, W. S. The Charge-State and Structural Stability of Peptides Conferred by Microsolvating Environments in Differential Mobility Spectrometry. *J. Am. Soc. Mass Spectrom.* **2021**, *32* (4), 956–968.

(44) Ieritano, C.; Hopkins, W. S. The Hitchhiker's Guide to Dynamic Ion-Solvent Clustering: Applications in Differential Ion Mobility Spectrometry. *Phys. Chem. Chem. Phys.* **2022**, *24* (35), 20594–20615.

(45) Haack, A.; Crouse, J.; Schlüter, F.-J.; Benter, T.; Hopkins, W. S. A First Principle Model of Differential Ion Mobility: The Effect of Ion-Solvent Clustering. *J. Am. Soc. Mass Spectrom.* **2019**, *30* (12), 2711–2725.

(46) Rawat, V. K.; Vidal-de-Miguel, G.; Hogan, C. J., Jr. Modeling Vapor Uptake Induced Mobility Shifts in Peptide Ions Observed with Transversal Modulation Ion Mobility Spectrometry-Mass Spectrometry. *Analyst* **2015**, *140* (20), 6945–6954.

(47) Reinecke, T.; Clowers, B. H. Implementation of a Flexible, Open-Source Platform for Ion Mobility Spectrometry. *HardwareX* **2018**, *4*, e00030.

(48) Morrison, K. A.; Siems, W. F.; Clowers, B. H. Augmenting Ion Trap Mass Spectrometers Using a Frequency Modulated Drift Tube Ion Mobility Spectrometer. *Anal. Chem.* **2016**, *88* (6), 3121–3129.

(49) Rappe, A. K.; Goddard, W. A., Iii. Charge Equilibration for Molecular Dynamics Simulations. *J. Phys. Chem.* **1991**, *95* (8), 3358–3363.

(50) Nosé, S. A Unified Formulation of the Constant Temperature Molecular Dynamics Methods. *J. Chem. Phys.* **1984**, *81* (1), 511–519.

(51) Evans, D. J.; Holian, B. L. The Nose–hoover Thermostat. *J. Chem. Phys.* **1985**, *83* (8),

4069–4074.
(52) Plimpton, S. Fast Parallel Algorithms for Short-Range Molecular Dynamics. *J. Comput. Phys.* **1995**, *117* (1), 1–19.
(53) Marchese, R.; Grandori, R.; Carloni, P.; Raugei, S. On the Zwitterionic Nature of Gas-Phase Peptides and Protein Ions. *PLoS Comput. Biol.* **2010**, *6* (5), e1000775.
(54) Sullards, M. C.; Reiter, J. A. Primary and Secondary Locations of Charge Sites in Angiotensin II (M + 2H)2+ Ions Formed by Electrospray Ionization. *J. Am. Soc. Mass Spectrom.* **2000**, *11* (1), 40–53.
(55) Tamadate, T.; Higashi, H.; Seto, T.; Hogan, C. J., Jr. Calculation of the Ion-Ion Recombination Rate Coefficient via a Hybrid Continuum-Molecular Dynamics Approach. *J. Chem. Phys.* **2020**, *152* (9), 094306.
(56) Wang, J.; Wolf, R. M.; Caldwell, J. W.; Kollman, P. A.; Case, D. A. Development and Testing of a General Amber Force Field. *J. Comput. Chem.* **2004**, *25* (9), 1157–1174.
(57) Tamadate, T.; Hogan, C. J., Jr. Silicon Nanocluster Anion-Argon Cation Recombination via Hybrid Continuum-Molecular Dynamics Calculations. *J. Aerosol Sci.* **2022**.
(58) Tamadate, T.; Higashi, H.; Hogan, C. J.; Seto, T. The Charge Reduction Rate for Multiply Charged Polymer Ions via Ion-Ion Recombination at Atmospheric Pressure. *Phys. Chem. Chem. Phys.* **2020**, *22* (43), 25215–25226.
(59) Edward A. Mason, E. W. M. *Transport Properties of Ions in Gases*; 1988.
(60) Alexander, W. M.; Ficarro, S. B.; Adelmant, G.; Marto, J. A. Multiplierz v2.0: A Python-Based Ecosystem for Shared Access and Analysis of Native Mass Spectrometry Data. *Proteomics* **2017**, *17* (15-16). https://doi.org/10.1002/pmic.201700091.
(61) Dongré, A. R.; Jones, J. L.; Somogyi, Á.; Wysocki, V. H. Influence of Peptide Composition, Gas-Phase Basicity, and Chemical Modification on Fragmentation Efficiency: Evidence for the Mobile Proton Model. *J. Am. Chem. Soc.* **1996**, *118* (35), 8365–8374.
(62) Jørgensen, T. J. D.; Gårdsvoll, H.; Ploug, M.; Roepstorff, P. Intramolecular Migration of Amide Hydrogens in Protonated Peptides upon Collisional Activation. *J. Am. Chem. Soc.* **2005**, *127* (8), 2785–2793.
(63) Stow, S. M.; Causon, T. J.; Zheng, X.; Kurulugama, R. T.; Mairinger, T.; May, J. C.; Rennie, E. E.; Baker, E. S.; Smith, R. D.; McLean, J. A.; *et al*. An Interlaboratory Evaluation of Drift Tube Ion Mobility-Mass Spectrometry Collision Cross Section Measurements. *Anal. Chem.* **2017**, *89* (17), 9048–9055.
(64) Jekel, C. F.; Venter, G. *PWLF: A Python Library for Fitting 1D Continuous Piecewise Linear Functions*; 2019. https://github.com/cjekel/piecewise_linear_fit_py.
(65) Lee, J. W.; Lee, H. H. L.; Davidson, K. L.; Bush, M. F.; Kim, H. I. Structural Characterization of Small Molecular Ions by Ion Mobility Mass Spectrometry in Nitrogen Drift Gas: Improving the Accuracy of Trajectory Method Calculations. *Analyst* **2018**, *143* (8), 1786–1796.
(66) Larriba, C.; Hogan, C. J. Ion Mobilities in Diatomic Gases: Measurement versus Prediction with Non-Specular Scattering Models. *J. Phys. Chem. A* **2013**, *117* (19), 3887–3901.
(67) Lalli, P. M.; Corilo, Y. E.; Fasciotti, M.; Riccio, M. F.; de Sa, G. F.; Daroda, R. J.; Souza, G. H. M. F.; McCullagh, M.; Bartberger, M. D.; Eberlin, M. N.; *et al*. Baseline Resolution of Isomers by Traveling Wave Ion Mobility Mass Spectrometry: Investigating the Effects of Polarizable Drift Gases and Ionic Charge Distribution. *J. Mass Spectrom.* **2013**, *48* (9), 989–997.
(68) Campuzano, I.; Bush, M. F.; Robinson, C. V.; Beaumont, C.; Richardson, K.; Kim, H.; Kim, H. I. Structural Characterization of Drug-like Compounds by Ion Mobility Mass Spectrometry: Comparison of Theoretical and Experimentally Derived Nitrogen Collision Cross Sections. *Anal. Chem.* **2012**, *84* (2), 1026–1033.
(69) Wu, T.; Derrick, J.; Nahin, M.; Chen, X.; Larriba-Andaluz, C. Optimization of Long Range Potential Interaction Parameters in Ion Mobility Spectrometry. *J. Chem. Phys.* **2018**, *148* (7), 074102.

(70) Robinson, E. W.; Williams, E. R. Multidimensional Separations of Ubiquitin Conformers in the Gas Phase: Relating Ion Cross Sections to H/D Exchange Measurements. *J. Am. Soc. Mass Spectrom.* **2005**, *16* (9), 1427–1437.

(71) Modzel, M.; Wollenberg, D. T. W.; Trelle, M. B.; Larsen, M. R.; Jørgensen, T. J. D. Ultraviolet Photodissociation of Protonated Peptides and Proteins Can Proceed with H/D Scrambling. *Anal. Chem.* **2021**, *93* (2), 691–696.

(72) Rand, K. D.; Adams, C. M.; Zubarev, R. A.; Jørgensen, T. J. D. Electron Capture Dissociation Proceeds with a Low Degree of Intramolecular Migration of Peptide Amide Hydrogens. *J. Am. Chem. Soc.* **2008**, *130* (4), 1341–1349.

(73) Arrington, J. V.; Straus, R. N.; Reynolds, P. F.; Poutsma, J. L.; Marzluff, E. M.; Poutsma, J. C. Gas-Phase Hydrogen Deuterium Exchange Behavior of Lysine and Its Homologs. *Int. J. Mass Spectrom.* **2012**, *330-332*, 200–206.

(74) Florance, H. V.; Stopford, A. P.; Kalapothakis, J. M.; McCullough, B. J.; Bretherick, A.; Barran, P. E. Evidence for α-Helices in the Gas Phase: A Case Study Using Melittin from Honey Bee Venom. *Analyst* **2011**, *136* (17), 3446–3452.

For Table of Contents Only: